Energy & Environmental Science

Unlocking the Potential of Cadmium Plating Chemistry for Low-Polarization, Long-Cycling, and Ultrahigh-Efficiency Aqueous Metal Batteries

Journal:	*Energy & Environmental Science*
Manuscript ID	EE-ART-04-2024-001615.R1
Article Type:	Paper
Date Submitted by the Author:	17-May-2024
Complete List of Authors:	Katiyar, Swati; University of Puerto Rico Chang, Songyang; University of Puerto Rico Rio Piedras Ullah, Irfan; University of Puerto Rico Rio Piedras, Department of Chemistry Hou, Wentao; University of Puerto Rico Rio Piedras, Department of Chemistry Conde-Delmoral, Amanda; University of Puerto Rico Rio Piedras, Department of Chemistry Qiu, Shen; University of Puerto Rico Rio Piedras, Department of Chemistry Morell, Gerardo; University of Puerto Rico Rio Piedras Wu, Xianyong; University of Puerto Rico Rio Piedras, Department of Chemistry

In the pursuit of next-generation energy solutions, aqueous metal batteries have emerged as competitive candidates, because of their potentially high safety, high energy, and low cost. While extensive research has focused on prominent transition metals such as zinc, our work delves into the overlooked cadmium metal, revealing its remarkable plating chemistry and unprecedented battery performance. Cadmium exhibits minimal polarization, extended lifespan, and exceptional plating efficiency, even under challenging conditions. Remarkably, these achievements are attained without complex electrolytes, intricate additives, or surface modifications, underscoring the intrinsic advantages of cadmium, such as its suitable redox potential and unique morphology. Moreover, our study demonstrates the viability of high-energy and high-rate cadmium batteries. By shedding light on the unexplored territory of cadmium-based redox chemistry, our work opens new avenues for designing high-performance metal batteries, offering significant implications for the advancement of energy storage solutions.

ARTICLE

Unlocking the Potential of Cadmium Plating Chemistry for Low-Polarization, Long-Cycling, and Ultrahigh-Efficiency Aqueous Metal Batteries

Received 00th January 20xx,
Accepted 00th January 20xx

DOI: 10.1039/x0xx00000x

Swati Katiyar,[#a] Songyang Chang,[#a] Irfan Ullah,[a] Wentao Hou,[a] Amanda Conde-Delmoral,[a] Shen Qiu,[a] Gerardo Morell,[b] and Xianyong Wu[*a]

Aqueous metal batteries represent a compelling avenue for energy storage solutions. Currently, research efforts are heavily concentrated on period 4 transition metals, starting from the prominent zinc to emerging candidates of iron, nickel, copper, and manganese. However, period 5 transition metals remain underexplored and poorly understood. Herein, we selected an underrepresented cadmium metal and investigated its fundamental plating chemistry, which showcases an unprecedented electrode performance, including low polarization (~5 mV), long lifespan (4000 hours, 5.5 months), and exceptional plating efficiency. Notably, the efficiency approaches unity (99.92%) at 1.0 mA cm^{-2} and 1.0 mAh cm^{-2}, and it retains 99.60-99.82% in more aggressive conditions (5-10 mAh cm^{-2}; 0.25-0.50 mA cm^{-2}). Surprisingly, such a performance is achieved without utilizing sophisticated electrolytes, additives, or surface treatments, which likely results from its suitable Cd^{2+}/Cd redox potential, high resistance to hydrogen evolution, and densely stacked plate-like morphology. High-energy, high-rate, and long-cycling cadmium batteries have also been demonstrated. Our work contributes novel insights into the design of high-performance metal batteries.

Introduction

Aqueous multivalent metal batteries have attracted growing attention for energy storage, owing to their potentially high energy, low cost, and nonflammability.[1-3] Presently, zinc metal batteries represent the mainstream option, but the parasitic electrode-electrolyte side reactions lead to insufficient Coulombic efficiency and inferior cycling stability.[4,5] Furthermore, zinc metal exhibits high propensity to dendrite growth,[6] leading to the short-circuit problem. To tackle these challenges, numerous approaches have been proposed, such as the development of sophisticated electrolytes[7-10] and functional additives or current collectors[11-14]. However, these methods may increase the cost of raw materials or battery manufacturing.

The pursuit of innovative metal plating chemistry is of critical importance, which not only enhances our fundamental understanding of element properties but also facilitates the development of advanced metal battery systems. Therefore, researchers have started examining alternative metal electrodes. In 2019, Ji *et al.* demonstrated a proof-of-concept of iron metal batteries, where the Fe^{2+}/Fe plating behavior and Fe^{2+} ion insertion reaction was studied.[15] Despite the moderate Fe plating efficiency (~91%), this work caused a paradigm shift for investigating post-zinc batteries. Later, researchers actively explored plating mechanisms of copper (Cu),[16-18] nickel (Ni),[19-21] and manganese (Mn)[22-24] for aqueous batteries, and many interesting results were achieved. Recently, a post-transition metal of tin (Sn) demonstrated its promise as a low-polarization and high-efficiency anode.[25] For instance, in an acidic electrolyte, the tin anode exhibited a moderate plating efficiency of ~98% at 2.0 mA cm^{-2}.[26] Regardless of these advances, rare attention has been paid to cadmium (Cd) plating chemistry, which constitutes a great knowledge gap. It also remains elusive whether Cd redox could bring new innovations for battery studies.

In fact, Cd possesses several appealing merits. Firstly, the standard Cd^{2+}/Cd electrode potential is -0.40 V *vs.* standard hydrogen electrode (SHE),[27] which is slightly above the hydrogen evolution potential at a pH=7 state (-0.413 V *vs.* SHE, **Figure 1a**).[28] This can ensure a maximal full cell voltage without causing appreciable hydrogen evolution side reactions. In comparison, the low-potential Fe, Zn, and Mn metals easily cause HER and low efficiency, while the high-potential Ni, Sn, and Cu metals inevitably compromise the full cell voltage. Secondly, in the catalysis field, Cd is well known for its high overpotential toward HER (**Figure 1b**),[29-31] which is on par with the prominent lead element. Therefore, the parasitic HER side reaction can be markedly suppressed, which will further contribute to a high plating efficiency. Thirdly, Cd exhibits a theoretical capacity of ~477 mAh g^{-1} (**Figure 1c** and **Table S1**), which is inferior to transition metals but surpasses the newly developed Sn anode (451 mAh g^{-1}).[26] Moreover, Cd has a high density of 8.65 g cm^{-3}, which compensates for its volumetric capacity (4125 mAh cm^{-3}).

[a] *Department of Chemistry, University of Puerto Rico-Rio Piedras Campus, San Juan, PR 00925-2537, USA*
[b] *Department of Physics, University of Puerto Rico-Rio Piedras Campus, San Juan, PR, 00925-2537, USA*
*Corresponding author: Dr. Xianyong Wu, xianyongwu2020@gmail.com
Electronic Supplementary Information (ESI) available: [details of any supplementary information available should be included here]. See DOI: 10.1039/x0xx00000x

ARTICLE

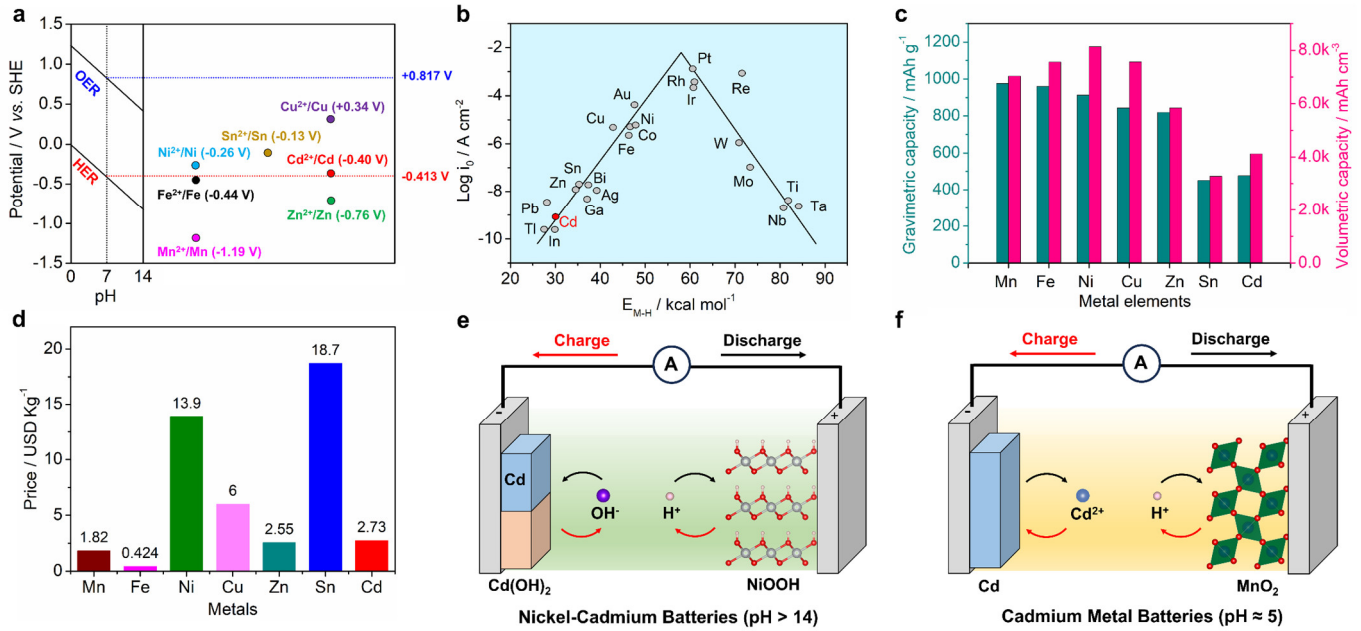

Figure 1. (a) The Pourbaix diagram of water and the standard electrode potentials of divalent M^{2+}/M couples, where M = Mn, Fe, Ni, Sn, Cu, Zn, and Cd; (b) The volcano plot of different metals toward HER, reproduced with permission from Ref. 29, copyright, 1972, Elsevier; (c) The gravimetric and volumetric capacities of divalent metals; (d) The elemental price of different metals; (e) The working mechanism of commercial Ni-Cd batteries in strong alkaline electrolytes (pH>14). The anode works on a Cd/$Cd(OH)_2$ conversion reaction, whereas the cathode operates on a proton insertion reaction in nickel oxide hydroxide (NiOOH); (f) The working mechanism of proposed cadmium metal batteries in mildly acidic Cd^{2+} electrolytes (pH≈5). The anode works on a Cd^{2+}/Cd plating mechanism, whereas the cathode operates on a proton insertion reaction in manganese dioxide (MnO_2).

Lastly, Cd is an inexpensive metal (2.73 USD/kg, **Figure 1d**), which rivals Zn (2.55 USD/kg) but is much cheaper than Ni (13.9 USD/kg), Cu (6.0 USD/kg), and Sn (18.7 USD/kg).[32] This would be the primary incentive for its applications in commercial nickel-cadmium (Ni-Cd) batteries (**Figure 1e**),[33-35]which offer higher energy than lead-acid batteries but much lower cost than nickel-metal-hydride batteries. However, Ni-Cd batteries utilize alkaline electrolytes and operate on the $Cd(OH)_2$/Cd conversion reaction instead of the Cd^{2+}/Cd plating chemistry.

In this work, we investigated the fundamental properties of cadmium plating chemistry and revealed its superior electrochemical performance (**Figure 1f**). Specifically, Cd exhibits an exceedingly low polarization of ~5 mV, a long cycling life of 4000 hours (5.5 months), and near-unity efficiency of ~99.92% at 1 mA cm^{-2} and 1 mAh cm^{-2}. At more stringent conditions, such as high capacity (5 and 10 mAh cm^{-2}) and low current (0.5 and 0.25 mA cm^{-2}), it still retains a high efficiency of 99.60-99.82%. We also explored the full cell applications of Cd metal batteries. The Cd-MnO_2 battery exhibited a high capacity of 310 mAh g^{-1} and a high energy of ~188 Wh kg^{-1}, whereas the Cd-$KNiFe(CN)_6$ hybrid battery showed an ultrahigh rate of 4000C (200 A g^{-1}) and stable cycling for >30,000 cycles.

Results and Discussion

To explore the Cd plating behavior, we utilized a conventional 1.0 mol L^{-1} $CdCl_2$ electrolyte, which shows a mild pH value of 4.91 and high ionic conductivity of 20.8 mS cm^{-1} (**Figure S1**). **Figure 2a** shows the typical cyclic voltammetry (CV) curve of the electrolyte in a three-electrode cell, where the working, counter, and reference electrode is titanium foil, Cd foil, and Ag/AgCl electrode (saturated KCl, +0.20 V *vs.* SHE), respectively. As shown, when the scanning potential reaches -0.64 V *vs.* Ag/AgCl, the cathodic current proliferates, which results from the Cd plating. During the positive scanning, the anodic peak occurs at -0.58 V *vs.* Ag/AgCl, indicating the Cd stripping. The average reaction potential is calculated as -0.61 V *vs.* Ag/AgCl, corresponding to -0.41 V *vs.* SHE, which agrees well with the standard Cd^{2+}/Cd potential (-0.40 V).

ARTICLE

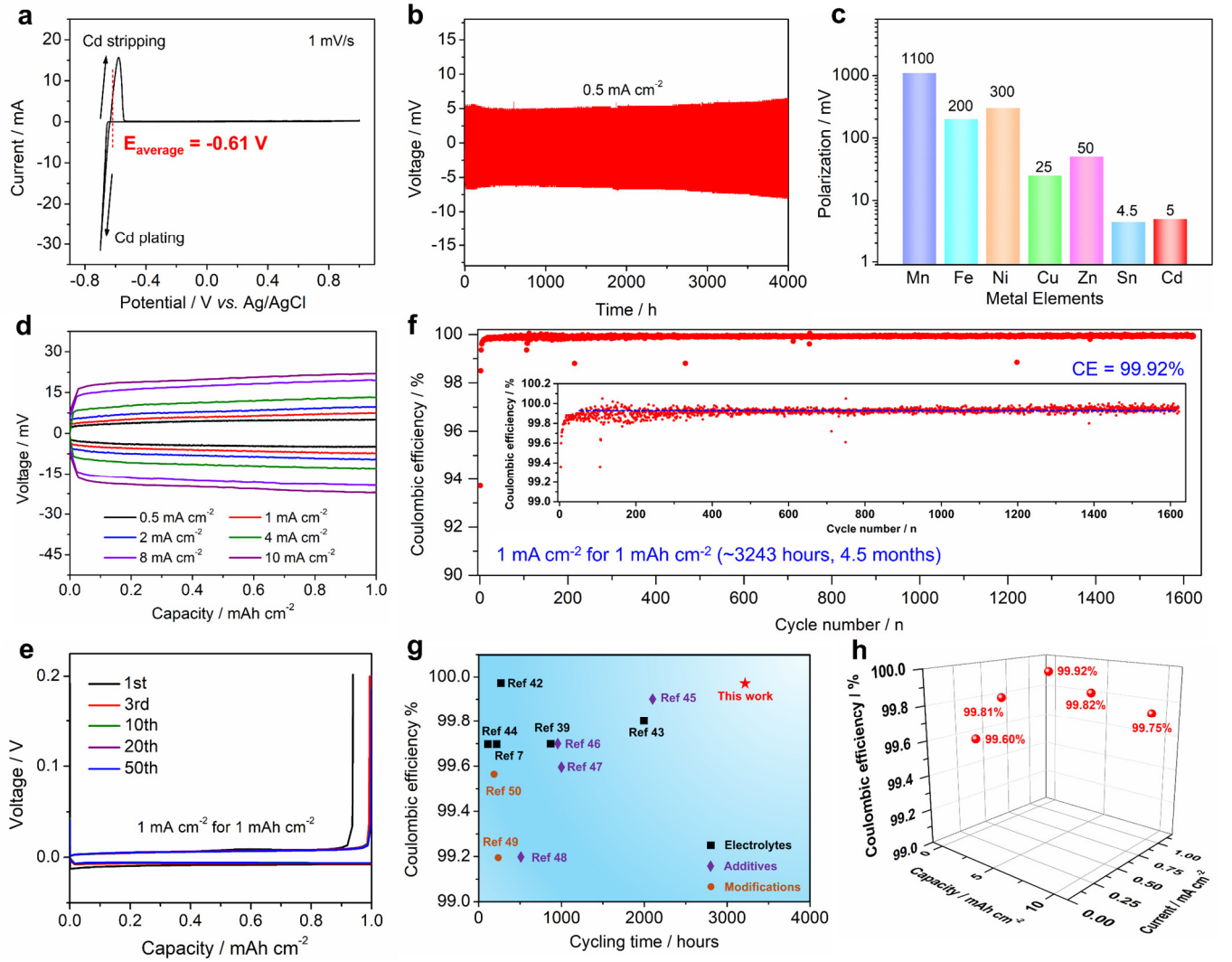

Figure 2. Electrochemical characterizations of the Cd metal in 1.0 M $CdCl_2$ electrolyte. (a) The CV curve of the electrolyte at 1.0 mV s^{-1}; (b) GCD curves of symmetrical Cd||Cd batteries at 0.5 mA cm^{-2} and 0.25 mAh cm^{-2}; (c) The polarization comparison between different divalent metals; (d) Rate performance of symmetrical Cd||Cd batteries; (e) GCD curves of the Cd||Cu battery at 1.0 mA cm^{-2} and 1.0 mAh cm^{-2}; (f) The plating efficiency during the long-term cycling, where the inset is an enlarged figure version; (g) The comparison between representative Zn batteries and Cd metal in terms of cycling time and efficiency; (h) A 3D plot to show the Cd plating efficiency at different current densities (0.25, 0.5, and 1 mA cm^{-2}) and capacities (1, 5, and 10 mAh cm^{-2}).

To evaluate the reaction kinetics and stability, we fabricated symmetrical Cd||Cd batteries (current: 0.5 mA cm^{-2}; capacity: 0.25 mAh cm^{-2}). The charge and discharge time is 1 hour for each cycle. **Figure 2b** displays Galvanostatic charge/discharge (GCD) curves, where a low polarization value of ~5 mV is observed. After a long cycling period of 4000 hours (5.5 months), there is no noticeable polarization increase or battery short-circuit, indicating a highly stable Cd plating process. **Figure S2** shows selected GCD curves at different testing cycles.

Of note, such small polarization is 1-2 orders of magnitude lower than transition metals at identical conditions,[36] such as Mn (1100 mV), Fe (200 mV), Ni (300 mV), Cu (25 mV), and Zn (50 mV), as shown in **Figure 2c** and **Figure S3**. Electrochemical impedance spectroscopy (EIS) finds that the symmetrical cell exhibits a marginal charge-transfer resistance of ~0.29 ohm (**Figure S4**), which suggests fast reaction kinetics and corroborates the small polarization. We thus tested the rate capability of symmetrical batteries. At higher currents of 1, 2, 4 and 8 mA cm^{-2} (**Figure 2d**), the polarization is ~6, 8, 12 and 18 mV, respectively. Even at 10 mA cm^{-2}, the polarization still remains low at 21 mV, which surpasses reported transition metals. Therefore, Cd metal holds promise for high-rate battery applications.

To further examine the Cd metal stability, we tested symmetrical batteries at larger currents and capacities. At a testing condition of 1.0 mA cm^{-2} and 0.25 mAh cm^{-2}, the Cd||Cd battery retains stable GCD curves for ~2900 hours (**Figure S5**). At 2.0 mA cm^{-2} current and 1.0 mAh cm^{-2} capacity, the Cd||Cd battery still shows smooth and well-defined GCD curves for ~2600 hours (**Figure S6**). These results collectively confirm the cycling stability of Cd metal.

Plating Coulombic efficiency (CE) is the most important metric for metal electrodes,[37-39] which directly determines the cycling life of metal batteries. We used a copper foil substrate for asymmetrical Cd||Cu batteries because it showed a better performance than the titanium foil (**Figure S7**). The plating efficiency was tested at 1.0 mA cm^{-2} and 1.0 mAh cm^{-2}. As shown in **Figure 2e**, the CE is 93.72% in the 1st cycle, which progressively rises to 98.50, 99.79, 99.83, and 99.90% in the 2nd, 10th, 20th, and 50th cycle, respectively. **Figure 2f** displays the cycling performance, where the average CE is as high as 99.92% over 1622 cycles, which is very close to unity (100%). Meanwhile, we underline that calendar life is another crucial parameter that reflects the cycling stability of aqueous batteries.[40,41] In this case, the cycling time is ~3243 hours (~4.5 months), and there is no battery failure or short-circuit, further validating the plating reversibility. It is noted that we plotted the efficiency in a very narrow range of 99-100.2% so that readers could better see the detailed efficiency values. These data points appear to be instable, but most of them fluctuate in a small scale of ±0.1%, which corroborates the high stability. **Figure S8** provides selected GCD curves of the Cd||Cu battery at 100th, 200th, 500th, 800th, and 1600th, which overlap well and have no obvious overpotential increase, further suggesting the high plating stability.

Surprisingly, such an exceptional efficiency and calendar life is achieved using a simple 1.0 M electrolyte and a pristine Cu foil substrate, which is rarely reported in the metal electrode context. For better understanding, we select some representative studies on Zn batteries and summarize their testing conditions and performances in **Table S2**. **Figure 2g** provides a comparison between the Zn and Cd in terms of plating efficiency and cycling time. Although Zn metal has realized high efficiencies (99.18-99.95%) and good cycling life (200-2200 hours) in asymmetrical batteries, it has to rely on the use of concentrated electrolytes,[7,39,42-44] functional additives,[45-48] or delicate surface treatments.[49,50] By contrast, Cd exhibits an extraordinary CE (99.93%) and cycling time (3243 hours) in a regular testing condition, which suggests a super low manufacturing cost. The comparison also underscores the excellent compatibility between the Cd^{2+}/Cd redox couple and aqueous electrolytes.

To further push the limit, we tested the Cd performance in harsher conditions. We fixed 1 mA cm^{-2} current but increased the capacity to 5 and 10 mAh cm^{-2}, which are sufficient in practical applications. Impressively, the average CE is 99.82% at 5 mAh cm^{-2} and 99.75% at 10 mAh cm^{-2} (**Figure S9**), respectively. Besides, these Cd||Cu batteries demonstrate a long calendar life of 998-2297 hours, and the CE value fluctuates in a small range of ±0.2%, indicating high reaction reversibility.

Aqueous metal batteries generally suffer from the parasitic HER side reaction,[51-53] which is a major reason for their inferior plating efficiency. To circumvent this issue, some researchers used very high current (5-50 mA cm^{-2}) to obscure HER, leading to "strategically" high efficiencies. However, HER will still reveal when batteries are at low-power or standby states. Thus, it is more valuable to obtain high efficiencies at lower current density. We fixed the capacity as 1 mAh cm^{-2} but decreased the current density accordingly. At a moderate current of 0.5 mA cm^{-2} (**Figure S10**), the average CE is 99.81% over 650 cycles (~2597 hours). At a low current of 0.25 mA cm^{-2}, Cd still maintains an impressively high CE of 99.60% (285 cycles, ~2274 hours, **Figure S10**). We further tested the efficiency at a very small current of 0.1 mA cm^{-2}, where each plating process takes 10 hours to complete. In this scenario, HER side reactions have sufficient time to play a role. Remarkably, the average CE is ~98.6% (84 cycles, ~1670 hours, **Figure S11**), which is close to 99.0%. **Figure 2h** summarizes the relationship between the plating current, capacity, and efficiency of the Cd metal.

We infer that such high Cd plating efficiency is closely related to its fundamental properties. Firstly, the Cd^{2+}/Cd redox couple enjoys a suitable potential of -0.40 V *vs.* SHE (**Figure 1a**), higher than its divalent metal siblings, such as Zn and Fe. Hence, Cd metal is thermodynamically more compatible with aqueous electrolytes, which minimizes HER side reactions. Indeed, at the same condition, Zn and Fe metals suffer from an inferior plating efficiency (92.2-97.9%, **Figure S12**) to Cd (99.60%, **Figure S10**).

Secondly, Cd features an immense overpotential toward hydrogen evolution (**Figure 1b**),[29-31, 54-56] which kinetically inhibits HER side reactions. Note that the $CdCl_2$ electrolyte is mildly acidic (pH~4.9), which renders a thermodynamic HER potential of -0.059*4.9= -0.289 V *vs.* SHE. Therefore, HER could theoretically take place because its potential exceeds the practical Cd plating potential (-0.41 V *vs.* SHE). Fortunately, the potential gap is merely 0.12 V, which can be easily overcome by kinetic parameters (0.25-1.0 mA cm^{-2}). To verify our hypothesis, we conducted linear scanning voltammetry (LSV) analysis on a mildly acidic 0.1 M ammonium chloride, using Cd and Cu foils for comparison. Of note, this NH_4Cl electrolyte has a similar pH value (~4.80) to 1 M $CdCl_2$ (~4.90), which can mimic the HER upon reduction. Besides, the Cu foil is the current collector used for Cd plating. As shown in **Figure 3a**, the Cd foil renders a much less current than Cu even at a very negative potential of -1.3 V *vs.* SHE, which validates the HER suppression capability of the Cd metal. The corrosion curve in **Figure S13** further reveals the minimal electrode-electrolyte side reaction and anti-HER capability of Cd metal.

Thirdly, the unique Cd plating morphology further contributes to its high efficiency. We selected four representative states for morphology observation (**Figure 3b**), namely plating 0.5 mAh cm^{-2} (point A), plating 1.0 mAh cm^{-2} (point B), stripping 0.5 mAh cm^{-2} (point C), and full stripping (point D).

At a moderate plating capacity (point A), the Cd metal appears as surface-flattened but irregular-shaped clusters, whose size varies between 30-80 μm (**Figure 3c**). Taking a closer look, we find that the Cd top comprises some smaller particles (marked in yellow circles), whereas the Cd base consists of many plate-like Cd chips that are closely stacked and densely packed (**Figure 3d**). **Figure 3e** shows a cross-sectional SEM image, which further confirms the joint particle-plate morphology. When plating capacity reaches 1.0 mAh cm^{-2} (point B), the overall Cd metals are better connected, and the deposit

size further enlarges to 50-100 μm (**Figure 3f**). At this stage, Cd particles on the top increase their population, and the Cd plates at the base increase their stacking layer numbers (**Figure 3g-h**). X-ray diffraction (XRD) and energy dispersive spectra (EDS) mapping analysis confirmed the high purity of these Cd deposits (**Figure S14-15**).

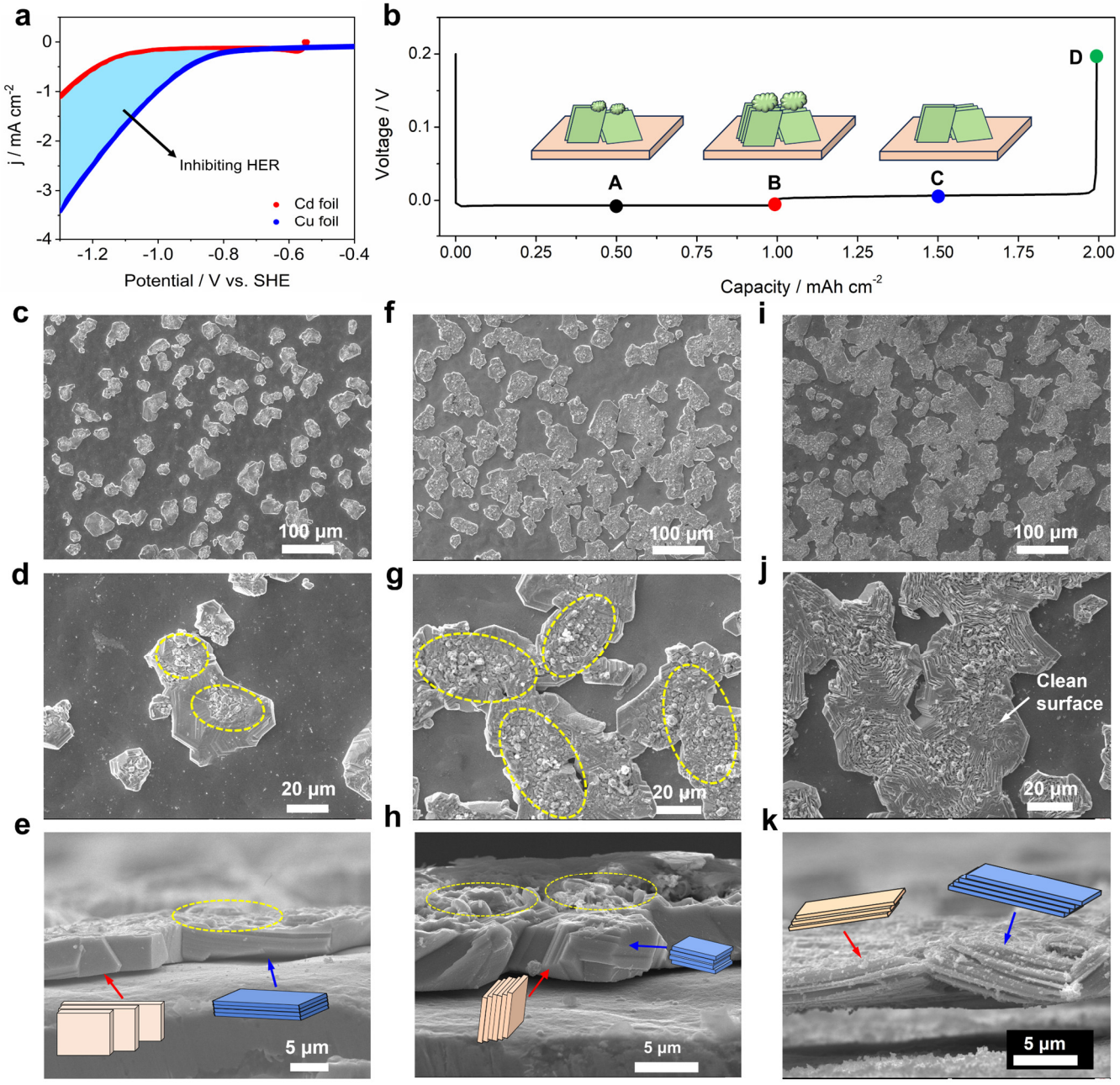

Figure 3. The HER resistance and morphology evolution of the Cd metal. (a) LSV curves of the Cd and Cu foils in 0.1 M NH_4Cl electrolyte; (b) A typical plating/stripping curve, the inset is a scheme to describe the morphology evolution; (c-e) Top-view and cross-sectional SEM images of Cd at a plating capacity of 0.5 mAh cm^{-2}; (f-h) Top-view and cross-sectional SEM images of Cd at a plating capacity of 1.0 mAh cm^{-2}; (i-k) Top-view and cross-sectional SEM images of Cd at a stripping capacity of 0.5 mAh cm^{-2}. The plating current is 1.0 mA cm^{-2}.

During the stripping process at 0.5 mAh cm^{-2} (point C), the Cd metal does not experience a noticeable particle size decrement, as compared in **Figure 3f** and **Figure 3i**. However, upon closer examination, we observe that the smaller particles on the top almost vanish, resulting in a relatively clean surface (**Figure 3j**). Meanwhile, the plate-stacking texture at the base becomes thinner and less dense (**Figure 3k**). This suggests that the stripping process starts from the top of Cd metal instead of its base. According to Li metal studies,[57,58] this top-stripping manner is advantageous for a complete stripping process; otherwise, residual metals may lose

ARTICLE

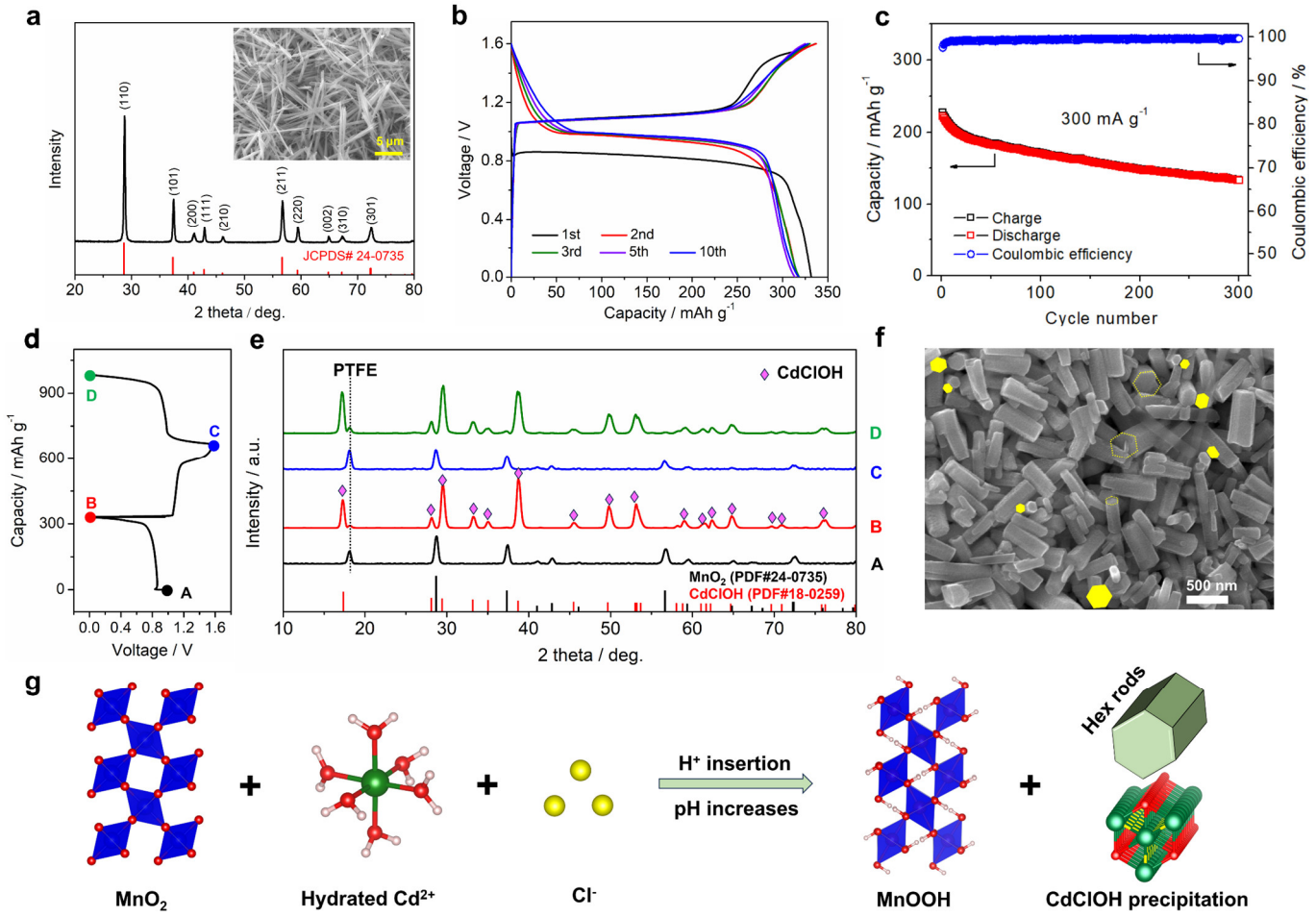

Figure 4. The characterization of the MnO2 material and the Cd||MnO_2 battery. (a) The XRD pattern of MnO_2, the inset is a SEM image; (b) GCD curves of the Cd||MnO_2 battery at 100 mA g^{-1}; (c) The cycling performance at 300 mA g^{-1}; (d) Selected states in a typical GCD cycle; (e) *Ex situ* XRD patterns of the MnO_2 electrodes; (f) A SEM image of the discharged MnO_2 electrode (point B); (g) The scheme of the MnO_2 battery reaction mechanism. The electrolyte is 1.0 M $CdCl_2$ + 0.1 M $MnCl_2$.

electron conduction with current collectors, thus becoming "dead" metals. **Figure S16** illustrates the difference between top stripping and base stripping. At the fully stripped stage (point D), all the plate-like metals disappear from the Cu substrate (**Figure S17**)

Notably, there is no dendrite growth during the entire plating/stripping cycle, and the Cd deposits are micron-sized particles and plates, which are closely packed to minimize the surface areas. This morphology is conducive to reducing electrode-electrolyte side reactions, which further reinforces the Coulombic efficiency.

We also tested its morphology at 5.0 and 10.0 mAh cm^{-2} capacity, where Cd retained a relatively flat and smooth surface without dendrites (**Figure S18-19**). After cycling in symmetrical batteries for 200 hours, the pristine Cd foil evolves into a plate-stacking morphology, which, again, resists the dendrite growth (**Figure S20**). These results explain well the outstanding efficiency and cycling life.

Encouraged by the superb Cd anode performance, we aim to develop a suitable cathode for Cd metal batteries. Herein, we selected a manganese dioxide (MnO_2) material, considering its high capacity (200-500 mAh g^{-1}) and low cost.[59-62] This material was prepared by a hydrothermal method, which adopts a tetragonal structure with a space group of P42/mnm (JCPSD # 24-0735, *β*-phase, **Figure 4a**). It shows a well-defined nanorod morphology, where the length is approximately 5-10 μm, and the diameter is a few hundred nanometers (**Figure 4a** inset). This material shows high chemical purity, as indicated by the EDS analysis (**Figure S21**).

We assembled Cd||MnO_2 batteries in a two-electrode cell configuration. The 1.0 M $CdCl_2$ electrolyte is added with 0.1 M $MnCl_2$, which can reinforce the cycling performance of MnO_2 based on the

common ion effect.[60] As shown in **Figure 4b**, the Cd||MnO_2 battery delivers a high discharge capacity of ~330 mAh g^{-1} and a flat discharge plateau at 0.84 V in the first cycle. Subsequently, the discharge capacity is stabilized at 310 mAh g^{-1}, and the discharge plateau increases to 1.0 V. The voltage elevation phenomena have been widely reported in Zn-MnO_2 batteries, due to the material morphology change and electrode activation.[60] Note that MnO_2 exhibits a theoretical capacity of 308 mAh g^{-1} via one-electron Mn^{4+}/Mn^{3+} redox, agreeing well with the practical discharge capacity.

The theoretical energy density for this Cd||MnO_2 battery is calculated as 188 Wh kg^{-1}, based on the cathode capacity (310 mAh g^{-1}), anode capacity (477 mAh g^{-1}), cell voltage (1.0 V), and a negative/positive (N/P) capacity ratio of 1:1 (see experimental section). This energy density is comparable to representative metal battery systems, as summarized in **Table S3**. If an N/P ratio of 2:1 is used, the energy density will be 135 Wh kg^{-1}. Assuming practical Cd||MnO_2 batteries have 40-50 wt.% mass burden from non-active components (current collectors, separators, electrolytes, and packages),[63,64] the final energy density may reach 67-80 Wh kg^{-1}, which exceeds that of commercial Ni-Cd batteries (40-60 Wh kg^{-1}).[33]

Besides the high energy, the MnO_2 battery demonstrates a reasonable rate and cycling capability. As displayed in **Figure S22**, it delivers a discharge capacity of ~310, 270, 240, 210, 188, and 171 mAh g^{-1} at 0.1, 0.2, 0.3, 0.5, 0.8, and 1.0 A g^{-1}, respectively. We carried out CV tests at different scanning rates (**Figure S22**) and fitted the relationship between the scanning rates and peak currents. According to the equation of $i=av^b$,[65] the b value is found ~0.5 for cathodic and anodic peaks, suggesting a diffusion-controlled insertion reaction. **Figure 4c** gives the cycling performance at 300 mA g^{-1} (~1C rate). After 300 cycles, the discharge capacity degrades from 222 to 133 mAh g^{-1}, which renders a moderate capacity retention of 60% and average Coulombic efficiency of 99.6%. **Figure S23** shows the selected GCD curves during cycling. The capacity fading is likely due to the manganese ion dissolution issue, as indicated by the dark precipitation on the separator (**Figure S24**). Future work will focus on the optimization of the MnO_2 morphology or electrolyte additives for better cycling stability.

To unveil the charge-storage mechanism of the MnO_2 cathode, we used *ex-situ* XRD techinques to investigate the structure evolution (**Figure 4d**). There is an additional peak at ~18.1° in the pristine MnO_2 electrode, due to the polytetrafluoroethylene binder (**Figure 4e**). At the fully discharged state, many new peaks emerge at 17.3, 28.1, 29.4, 33.2, 35.0, 38.7, 45.5, 49.8, and 53.1°, which can be well indexed to the hexagonal cadmium chloride hydroxide material (CdClOH, JCPDS#18-0259, a=b=3.671 Å, α=β=90°, γ=120°). This is a good implication of the proton insertion reaction,[59-62] which consumes H^+ ions from the $CdCl_2$ electrolyte (pH~4.9), consequently, increases the hydroxide concentration, and eventually leads to the Cd^{2+} salt precipitation.

SEM further consolidates the CdClOH precipitation. As shown in **Figure 4f** and **Figure S25**, many hexagonal rods show up in the discharged state, which results from the hexagonal crystal structure of CdClOH. EDS detects appreciable amounts of Cd and Cl elements plus less Mn element (**Figure S25**), suggesting that the MnOOH material is buried underneath the CdClOH precipitation. Cross-sectional SEM analysis discloses that this precipitation layer is approximately 80 μm thick (**Figure S26**), and the battery charge-transfer resistance increases from 12.9 to 17.5 Ω. Of note, the thick CdClOH deposits and relatively low-crystalline MnO_2 concurrently influenced the detection of the MnOOH phase by XRD. Thus, we used a micro-sized *β*-MnO_2 and partially washed away CdClOH deposits, and we successfully observed characteristic XRD peaks of MnOOH (PDF#12-0733, **Figure S27**).

At the fully charged state, all XRD peaks restore to their original positions (**Figure 4e**), suggesting the disappearance of CdClOH and the reformation of β-MnO_2. SEM analysis finds that the fully charged electrode does not contain any hexagonal rods (**Figure S28**), and the overall morphology consists of irregular and porous particles. It is possible that during the structure transformation, MnO_2 endures a certain degree of pulverization. At the second-cycle full discharge state, the CdClOH phase shows up again (**Figure 4e**), indicating a reversible reaction process. Meanwhile, CdClOH rods fully cover the MnO_2 electrode surface (**Figure S29**), although its hexagonal morphology becomes less obvious. We infer that the MnO_2 material provides initial "nucleation" sites for the CdClOH precipitation, thus affecting its final morphology (**Figure S30**). During the first discharge, the MnO_2 material has a well-defined nanorod morphology, whereas during the second discharge, MnO_2 has experienced substantial morphological changes due to the proton insertion/extraction reactions. The MnO_2 morphology change affects the nucleation of CdClOH, leading to its less obvious hexagonal morphology in the second cycle.

Based on these results, we conclude that the MnO_2 cathode works through a proton insertion mechanism, which likely forms a MnOOH discharge compound. Meanwhile, the H^+ insertion leads to the increment of OH^- concentration, which precipitates Cd^{2+} cations and Cl^- anions in the form of hexagonal CdClOH. The overall process is schematically illustrated in **Figure 4g**, and the pertinent chemical reactions are proposed as follows:

Ionization of water: $H_2O = H^+ + OH^-$

Redox reaction: $MnO_2 + H^+ + e^- = MnOOH$

Precipitation: $Cd^{2+} + OH^- + Cl^- = CdClOH$

Besides the high-energy Cd||MnO_2 battery, Cd metal is also feasible to construct high-power and long-cycling hybrid batteries. **Figure 5a** shows the working principle, where the anode operates on the reversible Cd^{2+}/Cd plating reaction, whereas the cathode preferentially hosts alternative cations, such as K^+. In this work, we selected a K-insertion Prussian blue analogue (PBA) of $KNi^{II}[Fe^{III}(CN)_6]$ (**Figure S31**) for demonstration purposes,[66] but alternative ions or materials can also be exploited in hybrid cells. This $KNi[Fe(CN)_6]$ cathode exhibits a moderate capacity of ~53 mAh g^{-1} and a reasonable voltage of ~1.2 V (**Figure 5b**). Comparative studies on GCD curves in different electrolytes confirm the K^+ insertion mechanism on the cathode (**Figure S32**).

Notably, this Cd hybrid battery exhibits an extraordinary rate capability. At 3, 20, 50, and 100 A g^{-1}, the discharge capacity is ~48, 46, 43, and 39 mAh g^{-1}, respectively. Even at an exceedingly high current of 200 A g^{-1}, which is approximately 4000 C rate, the

discharge capacity still retains 28 mAh g^{-1}, corresponding to 53% capacity utilization (**Figure 5c**). This likely results from the minimal charge-transfer resistance (**Figure S33**) and the nearly capacitive K^+ insertion process (**Figure S34**) in the large open $KNiFe(CN)_6$ structure. Furthermore, this hybrid battery demonstrates superior cycling stability (**Figure 5d**), where the capacity fades from 52 to 41 mAh g^{-1} after 32800 cycles, corresponding to a high-capacity retention of 78%. The selected GCD curves are provided in **Figure S35**. *Ex situ* XRD studies reveal that the volume change is only 3% during K^+ insertion (**Figure S36**), which accounts for its outstanding cycling stability.

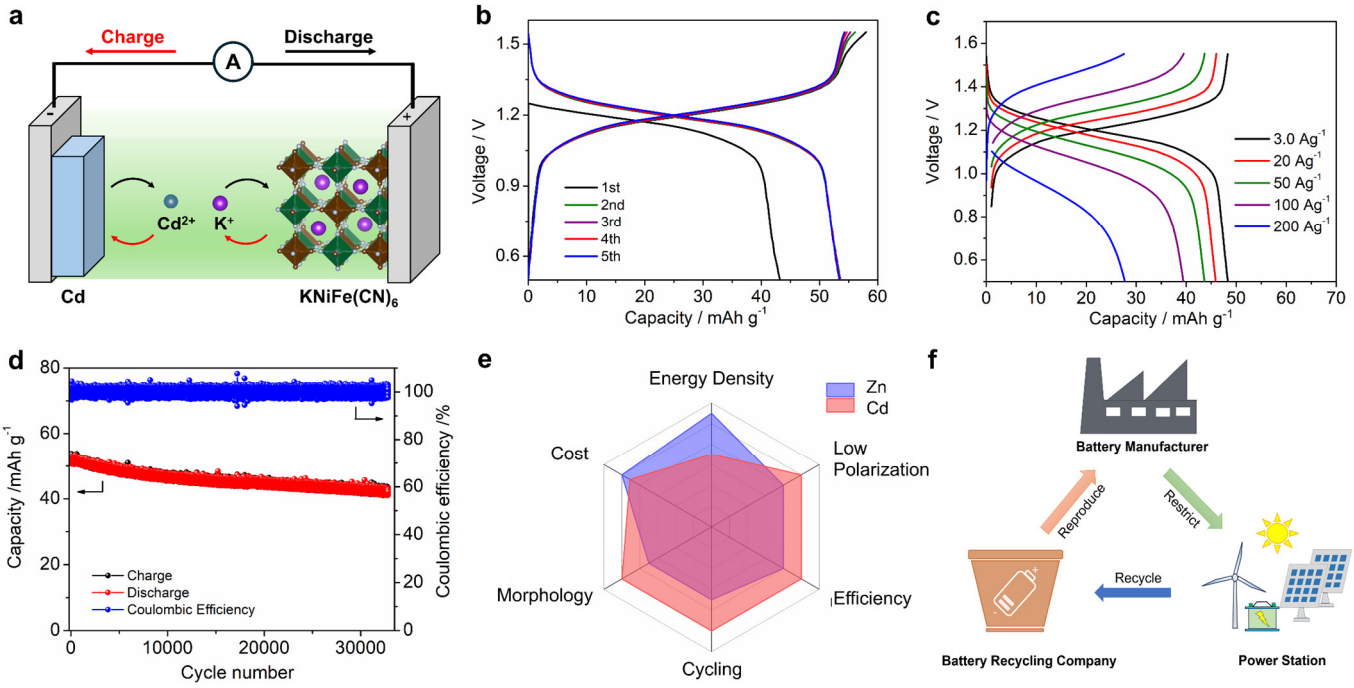

Figure 5. (a) The working mechanism of the hybrid battery of Cd ‖ $KNiFe(CN)_6$; (b) GCD curves of the hybrid battery in the electrolyte of 1 M $CdCl_2$ + 1 M KCl at 100 mA g^{-1}; (c) The rate performance; (d) The long-term cycling performance at 10 A g^{-1}; (e) The Radar plot comparison between the Zn and Cd metal; (f) A proposed application scenario of the Cd metal battery.

The Cd‖MnO_2 and Cd‖$KNiFe(CN)_6$ batteries demonstrate that the Cd metal is promising to build high-energy, high-rate, and long-cycling batteries. We also envision that many other promising cathode materials, such as sulfur, iodine, or vanadium oxides, can be explored to achieve better performance and unlock new redox chemistries.

We also would like to provide an overall comparison between this peculiar Cd metal and the prominent Zn metal (**Figure 5e**). Cd metal exhibits a lower capacity (477 mAh g^{-1}) and higher redox potential (-0.40 V *vs.* SHE) than Zn, which results in lower energy density. However, the higher Cd^{2+}/Cd potential offers some advantages in return, such as high compatibility with aqueous electrolytes (**Figure 1a**) and exceptional plating efficiencies. Moreover, Cd metal exhibits a closely stacked plate-like morphology, which effectively avoids the infamous dendrite growth issue, leading to extraordinary cycling stability. Additionally, Cd has a similarly low price compared with Zn, but its polarization is much smaller, leading to high-rate capabilities in hybrid batteries. It is worth mentioning that all these results are achieved without delicate material innovation or electrolyte engineering. Thus, even better Cd battery performance can be expected if we borrow the Zn battery research wisdom.

Unfortunately, the Cd element is toxic, which incurs some limitations for practical applications. The toxicity issue resembles that of commercial Ni-Cd batteries and Pb-acid batteries. Therefore, caution is needed when handling relevant Cd chemicals. However, it is crucial to recognize that Ni-Cd, Pb-acid, and Cd metal batteries represent distinct technologies, and they may find vastly different application areas. For instance, Ni-Cd batteries and Pb-acid can be sold to individual customers, which, if not disposed of properly, lead to environmental pollution.

To mitigate this issue, we propose a hypothetical application scenario for Cd metal batteries (**Figure 5f**). Cd metal batteries will be used for some specific and restricted cases only, such as stationary energy storage in rural areas. During operation, power station companies take responsibility for the battery monitoring and maintenance. When these batteries reach the end of cycling life, power station companies send them to a specific battery recycling enterprise. Subsequently, recycled materials will be used by the battery manufacturer to reproduce new Cd metal batteries. Hence, the “restrict, recycle, and reproduce” procedure forms a closed loop, which helps to minimize the toxicity and pollution issue. Noteworthy, Pb-acid batteries use the toxic lead element in the cathode (PbO_2) and anode (Pb) components, but more than 98% Pb has been successfully recycled and reproduced.[67] Ni-Cd batteries are still used in electric tools nowadays, owing to its super low cost and good energy and cycling life.

In parallel to rechargeable batteries, there are some efforts to investigate Cd based redox flow batteries, due to the cost, high-power, and plating reversibility attributes of Cd metals. For example, Zhao *et al.* reported a low-cost Fe/Cd redox flow battery,[68] which achieved a low capital cost of \$108 kWh^{-1} for 8-h energy storage and high energy efficiency of 80% at 120 mA cm^{-2}. Most recently, Li *et al.* demonstrated a Cd redox flow battery with a multiple-electron-transfer catholyte of I^-/IO_3^-, leading to predominantly high energy of 1200 Wh L^{-1} (based on the catholyte).[69] Along this line, the Cd toxicity issue could be partially offset by its superior battery performance (**Figure 5e**). Furthermore, with the advancement of battery manufacturing, sealing, and recycling technologies,[70] the toxicity issue can be further tolerated or addressed. It is also worth noting that gel-based electrolytes could be developed in light of aqueous Zn batteries, which will help to alleviate the liquid leakage issue. For instance, Yang *et al.* reported an aqueous gel electrolyte based on the crosslinked biomass-derived materials,[71] and they demonstrated Ah-scale zinc metal pouch cell without liquid leakage problem.

Lastly but more importantly, we note that this work is a scientific research endeavor to fill out the knowledge gap of Cd plating chemistry, instead of advocating commercialization of Cd metal batteries. Readers may differentiate the boundary between scientific research and practical applications. Indeed, through this study, we have unveiled unique properties of Cd redox chemistry, including minimal polarization, ultrahigh efficiency, resistance to hydrogen evolution, and distinctive plate-stacking morphology. These insights significantly contribute to our fundamental understanding of metal plating mechanisms, potentially catalyzing the development of high-performance metal batteries.

Conclusions

In conclusion, we investigated the fundamental properties of Cd plating chemistry and demonstrated its promise as a low-polarization, long-cycling, and ultrahigh-efficiency metal anode for aqueous multivalent batteries. At various testing conditions (0.25-1 mA cm^{-2}; 1-10 mAh cm^{-2}), it exhibits an incredibly high efficiency of 99.60-99.92% in a regular 1 M $CdCl_2$ electrolyte, which far exceeds most metal electrodes. This performance is closely related to its intrinsic properties, including a suitable redox potential, high HER resistance, and desirable plating morphology. We also explored the full cell applications, where high-energy, high-rate, and long-cycling batteries were demonstrated.

Author Contributions

[#]Swati Katiyar and [#]Songyang Chang contributed equally to this work. All authors have given the permission for the final version of this manuscript. Conceptualization: X. Wu; Data curation and formal analysis: S. Katiyar, S. Chang, I. Ullah, W. Hou, A. Conde-Delmoral; Visualization: S. Qiu and X. Wu; Resources: G. Morell and X. Wu; Writing – original draft, review, and editing: X. Wu.

Conflicts of interest

There are no conflicts to declare.

Acknowledgements

This work is financially supported by the NSF Center for the Advancement of Wearable Technologies (Grant No. 1849243) and NASA MIRO PR-SPRInT (grant no. 80NSSC19M0236).

Notes and references

1 D. Chao, W. Zhou, F. Xie, C. Ye, H. Li, M. Jaroniec and S.-Z. Qiao, *Sci. Adv.*, 2020, **6**, eaba4098.
2 X. Tang, D. Zhou, B. Zhang, S. Wang, P. Li, H. Liu, X. Guo, P. Jaumaux, X. Gao, Y. Fu, C. Wang, C. Wang and G. Wang, *Nat. Commun.*, 2021, **12**, 2857.
3 Z. Pan, X. Liu, J. Yang, X. Li, Z. Liu, X. J. Loh and J. Wang, *Adv. Energy Mater.*, 2021, **11**, 2100608.
4 X. Jia, C. Liu, Z. G. Neale, J. Yang and G. Cao, *Chem. Rev.*, 2020, **120**, 7795-7866.
5 B. Tang, L. Shan, S. Liang and J. Zhou, *Energy Environ. Sci.*, 2019, **12**, 3288-3304.
6 V. C. Ho, H. Lim, M. J. Kim and J. Mun, *Chem. –Asian J.*, 2022, **17**, e202200289.
7 F. Wang, O. Borodin, T. Gao, X. Fan, W. Sun, F. Han, A. Faraone, J. A. Dura, K. Xu and C. Wang, *Nat. Mater.*, 2018, **17**, 543.
8 L. Cao, D. Li, E. Hu, J. Xu, T. Deng, L. Ma, Y. Wang, X.-Q. Yang and C. Wang, *J. Am. Chem. Soc.*, 2020, **142**, 21404-21409.
9 C. Zhang, J. Holoubek, X. Wu, A. Daniyar, L. Zhu, C. Chen, D. P. Leonard, I. A. Rodríguez-Pérez, J.-X. Jiang and C. Fang, *Chem. Commun.*, 2018, **54**, 14097-14099.
10 W. Xu, J. Li, X. Liao, L. Zhang, X. Zhang, C. Liu, K. Amine, K. Zhao and J. Lu, *J. Am. Chem. Soc.*, 2023, **145**, 22456-22465.
11 Q. Zhang, J. Luan, L. Fu, S. Wu, Y. Tang, X. Ji and H. Wang, *Angew. Chem. Int. Ed.*, 2019, **58**, 15841-15847.
12 B. Li, K. Yang, J. Ma, P. Shi, L. Chen, C. Chen, X. Hong, X. Cheng, M. C. Tang and Y. B. He, *Angew. Chem. Int. Ed.*, 2022, **61**, e202212587.
13 L. Zhou, F. Yang, S. Zeng, X. Gao, X. Liu, X. Cao, P. Yu and X. Lu, *Adv. Funct. Mater.*, 2022, **32**, 2110829.
14 M. Fayette, H. J. Chang, X. Li and D. Reed, *ACS Energy Letters*, 2022, **7**, 1888-1895.
15 X. Wu, A. Markir, Y. Xu, C. Zhang, D. P. Leonard, W. Shin and X. Ji, *Adv. Funct. Mater.*, 2019, **29**, 1900911.
16 G. Liang, F. Mo, Q. Yang, Z. Huang, X. Li, D. Wang, Z. Liu, H. Li, Q. Zhang and C. Zhi, *Adv. Mater.*, 2019, **31**, 1905873.
17 H. Cai, S. Bi, R. Wang, L. Liu and Z. Niu, *Angew. Chem. Int. Ed.*, 2022, **61**, e202205472.
18 X. Wu, A. Markir, L. Ma, Y. Xu, H. Jiang, D. P. Leonard, W. Shin, T. Wu, J. Lu and X. Ji, *Angew. Chem. Int. Ed.*, 2019, **58**, 12640-12645.
19 J. Zhao, X. Yang, S. Li, N. Chen, C. Wang, Y. Zeng and F. Du, *CCS Chemistry*, 2021, **3**, 2498-2508.
20 S. Li, X. Yang, X. Li, Z. Wei, M. Li, F. Hu, Y. Xie, X. Meng, C. Wang and G. Chen, *Chem. Eng. J.*, 2021, **413**, 127441.
21 M. Wang, Y. Meng, P. Gao, K. Li, Z. Liu, Z. Zhu, M. Ali, T. Ahmad, N. Chen and Y. Yuan, *Adv. Mater.*, 2023, **35**, 2305368.
22 S. Bi, S. Wang, F. Yue, Z. Tie and Z. Niu, *Nat. Commun.*, 2021, **12**, 6991.
23 Q. Yang, X. Qu, H. Cui, X. He, Y. Shao, Y. Zhang, X. Guo, A. Chen, Z. Chen and R. Zhang, *Angew. Chem. Int. Ed.*, 2022, **61**, e202206471.
24 M. Wang, Y. Meng, Y. Xu, N. Chen, M. Chuai, Y. Yuan, J. Sun, Z. Liu, X. Zheng and Z. Zhang, *Energy Environ. Sci.*, 2023, **16**, 5284-5293.

25 W. Zhou, M. Song, P. Liang, X. Li, X. Liu, H. Li, T. Zhang, B. Wang, R. Zhao and Z. Zhao, *J. Am. Chem. Soc.*, 2023, **145**, 10880-10889.
26 H. Zhang, D. Xu, F. Yang, J. Xie, Q. Liu, D.-J. Liu, M. Zhang, X. Lu and Y. S. Meng, *Joule*, 2023, **7**, 971-985.
27 S. G. Bratsch, *J. Phys. Chem. Ref. Data*, 1989, **18**, 1-21.
28 J.-Y. Luo, W.-J. Cui, P. He and Y.-Y. Xia, *Nat. Chem.*, 2010, **2**, 760-765.
29 S. Trasatti, *J. Electroanal. Chem. Interfacial Electrochem.*, 1972, **39**, 163-184.
30 P. Quaino, F. Juarez, E. Santos and W. Schmickler, *Beilstein J. Nanotechnol.*, 2014, **5**, 846-854.
31 A. R. Zeradjanin, J. P. Grote, G. Polymeros and K. J. J. Mayrhofer, *Electroanalysis*, 2016, **28**, 2256-2269.
32 Prices of chemical elements. *Wikipedia*. https://en.wikipedia.org/wiki/Prices_of_chemical_elements (accessed on Jan 17th, 2024)
33 Z. Yang, J. Zhang, M. C. Kintner-Meyer, X. Lu, D. Choi, J. P. Lemmon and J. Liu, *Chem. Rev.*, 2011, **111**, 3577-3613.
34 F. Putois, *J. Power Sources*, 1995, **57**, 67-70.
35 E. Blumbergs, V. Serga, E. Platacis, M. Maiorov and A. Shishkin, *Metals*, 2021, **11**, 1714.
36 S. Chang, J. F. F. Gomez, S. Katiyar, G. Morell and X. Wu, *J. Am. Chem. Soc.*, 2023, **145**, 24746-24754.
37 J. Xiao, Q. Li, Y. Bi, M. Cai, B. Dunn, T. Glossmann, J. Liu, T. Osaka, R. Sugiura and B. Wu, *Nat. Energy*, 2020, **5**, 561-568.
38 B. D. Adams, J. Zheng, X. Ren, W. Xu and J. G. Zhang, *Adv. Energy Mater.*, 2018, **8**, 1702097.
39 H. Jiang, L. Tang, Y. Fu, S. Wang, S. K. Sandstrom, A. M. Scida, G. Li, D. Hoang, J. J. Hong and N.-C. Chiu, *Nat. Sustain.*, 2023, 1-10.
40 X. Ji and L. F. Nazar, *Nat. Sustain.*, 2024, 1-2.
41 Y. Xu, X. Wu and X. Ji, *Small Struct.*, 2021, **2**, 2000113.
42 C. Zhang, W. Shin, L. Zhu, C. Chen, J. C. Neuefeind, Y. Xu, S. I. Allec, C. Liu, Z. Wei, A. Daniyar, J.-X. Jiang, C. Fang, P. Alex Greaney and X. Ji, *Carbon Energy*, 2021, **3**, 339-348.
43 L. Cao, D. Li, T. Pollard, T. Deng, B. Zhang, C. Yang, L. Chen, J. Vatamanu, E. Hu and M. J. Hourwitz, *Nat. Nanotech.*, 2021, **16**, 902-910.
44 L. Cao, D. Li, F. A. Soto, V. Ponce, B. Zhang, L. Ma, T. Deng, J. M. Seminario, E. Hu and X. Q. Yang, *Angew. Chem. Int. Ed.*, 2021, **60**, 18845-18851.
45 R. Zhao, H. Wang, H. Du, Y. Yang, Z. Gao, L. Qie and Y. Huang, *Nat. Commun.*, 2022, **13**, 3252.
46 J. Hao, L. Yuan, C. Ye, D. Chao, K. Davey, Z. Guo and S. Z. Qiao, *Angew. Chem. Int. Ed.*, 2021, **60**, 7366-7375.
47 S. Ilic, M. J. Counihan, S. N. Lavan, Y. Yang, Y. Jiang, D. Dhakal, J. Mars, E. N. Antonio, L. Kitsu Iglesias and T. T. Fister, *ACS Energy Lett.*, 2023, **9**, 201-208.
48 X. Zhang, J. Chen, H. Cao, X. Huang, Y. Liu, Y. Chen, Y. Huo, D. Lin, Q. Zheng and K. h. Lam, *Small*, 2023, **19**, 2303906.
49 S. Jiao, J. Fu, M. Wu, T. Hua and H. Hu, *ACS Nano*, 2021, **16**, 1013-1024.
50 X. Xie, S. Liang, J. Gao, S. Guo, J. Guo, C. Wang, G. Xu, X. Wu, G. Chen and J. Zhou, *Energy Environ. Sci.*, 2020, **13**, 503-510.
51 Y. Sui and X. Ji, *Chem. Rev.*, 2021, **121**, 6654-6695.
52 L. Ma, M. A. Schroeder, O. Borodin, T. P. Pollard, M. S. Ding, C. Wang and K. Xu, *Nat. Energy*, 2020, **5**, 743-749.
53 C.-C. Kao, C. Ye, J. Hao, J. Shan, H. Li and S.-Z. Qiao, *ACS nano*, 2023, **17**, 3948-3957.
54 I. A. Ammar and M. Hassanein, *J. Phys. Chem.*, 1960, **64**, 558-560.
55 Y. Liu, S. Gao, R. Holze and A. K. Shukla, *J. Electrochem. Soc.*, 2017, **164**, A3858.
56 R. R. Adžić, M. D. Spasojević and A. R. Despić, *Electrochim. Acta*, 1979, **24**, 569-576.
57 F. N. Jiang, S. J. Yang, H. Liu, X. B. Cheng, L. Liu, R. Xiang, Q. Zhang, S. Kaskel and J. Q. Huang, *SusMat*, 2021, **1**, 506-536.
58 D. Lin, Y. Liu and Y. Cui, *Nat. Nanotechnol.*, 2017, **12**, 194-206.
59 X. Liu, J. Yi, K. Wu, Y. Jiang, Y. Liu, B. Zhao, W. Li and J. Zhang, *Nanotechnology*, 2020, **31**, 122001.
60 H. Pan, Y. Shao, P. Yan, Y. Cheng, K. S. Han, Z. Nie, C. Wang, J. Yang, X. Li and P. Bhattacharya, *Nat. Energy*, 2016, **1**, 16039.
61 D. Chao, W. Zhou, C. Ye, Q. Zhang, Y. Chen, L. Gu, K. Davey and S. Z. Qiao, *Angew. Chem. Int. Ed.*, 2019, **58**, 7823-7828.
62 W. Liu, X. Zhang, Y. Huang, B. Jiang, Z. Chang, C. Xu and F. Kang, *J. Energy Chem.*, 2021, **56**, 365-373.
63 J. Betz, G. Bieker, P. Meister, T. Placke, M. Winter and R. Schmuch, *Adv. Energy Mater.*, 2019, **9**, 1803170.
64 C. Niu, H. Lee, S. Chen, Q. Li, J. Du, W. Xu, J.-G. Zhang, M. S. Whittingham, J. Xiao and J. Liu, *Nat. Energy*, 2019, **4**, 551-559.
65 V. Augustyn, J. Come, M. A. Lowe, J. W. Kim, P.-L. Taberna, S. H. Tolbert, H. D. Abruña, P. Simon and B. Dunn, *Nat. Mater.*, 2013, **12**, 518-522.
66 C. D. Wessells, S. V. Peddada, R. A. Huggins and Y. Cui, *Nano Lett.*, 2011, **11**, 5421-5425.
67 M. Li, J. Liu and W. Han, *Waste Manag. Res.*, 2016, **34**, 298-306.
68 Y. Zeng, T. Zhao, X Zhou, L. Wei, H. Jiang, *J. Power Sources*, 2016, **330**, 55-60.
69 C. Xie, C. Wang, Y. Xu, T. Li, Q. Fu, X. Li, *Nat. Energy*, 2024, DOI: 10.1038/s41560-024-01515-9.
70 O. Velázquez-Martínez, J. Valio, A. Santasalo-Aarnio, M. Reuter and R. Serna-Guerrero, *Batteries*, 2019, **5**, 68.
71 F. Wang, J. Zhang, H. Lu, H. Zhu, Z. Chen, L. Wang, J. Yu, C. You, W. Li, J. Song, Z. Weng, C. Yang, Q. Yang, *Nat. Commun.*, 2023, **14**, 4211.